Bulletin of the Seismological Society of America, Vol. 95, No. 3, pp. 779–799, June 2005, doi: 10.1785/0120040112

The Mantle Magnitude M_m and the Slowness Parameter Θ: Five Years of Real-Time Use in the Context of Tsunami Warning

by Stuart A. Weinstein and Emile A. Okal

Abstract We study a database of more than 119,000 measurements of the mantle magnitude M_m introduced by Okal and Talandier (1989), obtained since 1999 as part of the operational procedures at the Pacific Tsunami Warning Center. The performance of this method is significantly affected by the seismic instrumentation at the recording station, with the very-broadband STS-1 and KS54000 systems offering the lowest residuals between measured values of M_m and those predicted from the Harvard Centroid Moment Tensor (CMT) catalog, and also by the period at which spectral amplitudes are measured, with the best results between 70 and 250 sec. With such mild restrictions, estimates of seismic moments can be obtained in real time by retaining either the maximum value of M_m measured on each record, or its average over the various mantle frequencies, with the resulting residuals, on the order of 0.1 ± 0.2 moment magnitude units. M_m deficiencies in the case of the two large earthquakes of Peru (2001) and Hokkaido (2003) are attributed to azimuthal bias from an excess of stations (principally in North America) in directions nodal for the focal mechanism and directivity patterns. We further study a group of more than 3000 measurements of the energy-to-moment ratio Θ introduced by Newman and Okal (1998), which allows the real-time identification of teleseismic sources violating scaling laws and, in particular, of so-called "tsunami earthquakes." The use of a sliding window of analysis in the computation of Θ allows the separation of "late earthquakes," characterized by a delayed but fast moment release, from truly slow earthquakes. Many such events are recognized, notably on major oceanic and continental strike-slip faults.

Introduction and Background

We present detailed analyses of a large dataset resulting from implementation, as part of the operational procedures of the Pacific Tsunami Warning Center (PTWC), of the real-time calculation of the mantle magnitude M_m and of the slowness parameter Θ, as defined and introduced by Okal and Talandier (1989) and Newman and Okal (1998), respectively. During the past five years, more than 119,000 individual measurements of M_m and 3000 values of Θ have been computed through automated algorithms. These values contribute to the estimation of the source characteristic of distant earthquakes in the framework of the real-time assessment of their tsunamigenic potential. This study offers a progress report on the performance of the algorithms and, in particular, discusses the influence of instrumentation at the various reporting stations.

As the final revision of this article was being prepared, the occurrence of the great Sumatra earthquake on 26 December 2004 provided an opportunity to extend the concepts of M_m and Θ to a range of magnitudes unexplored for the past 40 years. Preliminary results on the Sumatra earthquake are given in the Appendix.

The Magnitude M_m

The mantle magnitude M_m was initially developed by Okal and Talandier (1989) and implemented at the Papeete, Tahiti, tsunami center (Centre Polynésien de Prévention des Tsunamis, CPPT), where it has been used routinely for more than a decade in the context of tsunami warning. It was introduced to alleviate the saturation of the classical surface-wave magnitude M_s at values of ~8.3, which is caused by destructive interference effects when the source duration of large earthquakes becomes significantly longer than the fixed period (20 sec) at which M_s is measured (Geller, 1976). In particular, M_s is of little use in the context of tsunami warning, because it fails to separate merely large events with little or no transoceanic tsunami risk (approximately $M_0 = 10^{28}$ dyne cm) from those truly gigantic ones, such as the

1960 Chilean, 1964 Alaskan, and now 2004 Sumatran earthquakes ($M_0 > 10^{29}$ dyne cm), capable of exporting death and destruction to distant shores. Consequently, the main idea behind M_{m} was to make measurements at variable periods, which for large events means in the window of mantle surface waves, anywhere between 50 and 300 sec, while keeping the concept of magnitude, that is, a "quick-and-dirty" real-time one-station measurement ignoring source details such as focal mechanism and exact focal depth.

In practice, the measurement is made on each spectral component of the Rayleigh wave, and M_{m} is computed as

$$M_{\mathrm{m}} = \log_{10} X(\omega) + C_S + C_D - 0.90 \qquad (1)$$

where $X(\omega)$ is the spectral amplitude of ground motion in μm*s, C_D is a distance correction compensating for geometrical spreading on the spherical Earth and anelastic attenuation during propagation, and C_S is a frequency-dependent source correction, compensating for the variable excitation of Rayleigh waves of different periods by a seismic dislocation of unit moment. In keeping with the philosophy of a magnitude scale, C_S is computed for an average focal mechanism and source depth. The exact expressions of C_S and C_D are justified theoretically (as well as the locking constant $C_0 = -0.90$ in equation 1) in Okal and Talandier (1989); M_{m} is then expected to represent the seismic moment M_0 of the earthquake through:

$$M_{\mathrm{m}} = \log_{10} M_0 - 20 \qquad (2)$$

where M_0 is in dyne cm. The performance of M_m was tested initially on a dataset of 256 records by Okal and Talandier (1989). Defining a logarithmic residual,

$$r = M_{\mathrm{m}} - \log_{10} M_0 + 20, \qquad (3)$$

with respect to the published value M_0, they obtained an average value $\bar{r}$ and a standard deviation σ of 0.14 and 0.25 logarithmic units, respectively. A few years later, and after the implementation of an automatic procedure at CPPT, Hyvernaud *et al.* (1993) obtained $\bar{r} = 0.07$ and $\sigma = 0.22$ for a dataset of 474 measurements. A series of later studies extended the concept to Love waves (Okal and Talandier, 1990), nonshallow events (Okal, 1990), and historical earthquakes (Okal, 1992a,b) and verified its performance for truly gigantic earthquakes (Okal and Talandier, 1991) and in the regional field (Talandier and Okal, 1992; Schindelé *et al.*, 1995).

The Parameter Θ

One of the challenges of tsunami warning is to recognize in real time the so-called "tsunami earthquakes," defined by Kanamori (1972) as events whose tsunami is significantly larger than expected from their seismic waves. Classical examples are the 1896 Sanriku and 1946 Aleutian earthquakes, and more recently the 1992 Nicaragua, 1994 Java, and 1996 Chimbote, Peru, events. A general consensus from several careful studies (Fukao, 1979; Kanamori and Kikuchi, 1993; Polet and Kanamori, 2000) is that tsunami earthquakes involve an anomalously slow propagation of the rupture along the fault (at velocities as low as ~1 km/sec), resulting in destructive interference for all periods characteristic of seismic waves, including mantle ones. Such slow rupture velocities have been attributed either to rupture in a sedimentary wedge featuring deficient mechanical properties, as advocated by Fukao (1979) in the Kuriles, or to a jerky rupture process along a corrugated plate boundary in a sediment-starved interface (Tanioka *et al.*, 1997), such as in Nicaragua (Polet and Kanamori, 2000). Finally, those events whose tsunamis were primarily caused by an independently triggered landslide (e.g., Papua New Guinea, 1998 [Synolakis *et al.*, 2002]) are generally not considered genuine "tsunami earthquakes."

In this framework, Newman and Okal (1998) introduced the concept of the estimated seismic energy E^E released into generalized body waves by an earthquake source, by adapting the calculations of Boatwright and Choy (1986) to an *a priori* unknown focal mechanism and source depth. The comparison between estimated energy and seismic moment through the parameter

$$\Theta = \log_{10} \frac{E^E}{M_0} \qquad (4)$$

provides an evaluation of the slowness of the earthquake rupture. Arguments based on scaling laws (Geller, 1976; Scholz, 1982; Vassiliou and Kanamori, 1982) would predict $\Theta = -4.90$, a value supported by the datasets analyzed both by Boatwright and Choy (1986) and Newman and Okal (1998). By contrast, documented tsunami earthquakes feature Θ values deficient by 1 to 1.4 logarithmic units. Thus, Θ appears as a potential real-time identifier of tsunami earthquakes; note that it can be regarded as a modern-day extension of the classical $m_{\mathrm{b}} : M_{\mathrm{s}}$ discriminant, used extensively for the identification of nuclear explosions (e.g., Marshall and Basham, 1972). In the near field, Shapiro *et al.* (1998) introduced a method conceptually reminiscent of the computation of Θ by examining the ratio of high frequency to total energy in a regional seismogram to identify earthquake source slowness. However, although the latter can enhance tsunami excitation, tsunamis inflicting significant damage in the near field have been generated by earthquakes not featuring any particular source slowness (e.g., Flores, Indonesia, 1992).

In this general framework, the present study reports on the recent implementation at the Pacific Tsunami Warning Center (PTWC) of the calculation of both the magnitude M_{m} and the slowness parameter Θ, as part of the routine, real-time assessment of tsunami risk from distant earthquakes.

Implementation at PTWC

Mantle magnitudes are computed at PTWC from broadband data continuously sent in real time over the U.S. Geological Survey *Earthworm* data-distribution system. The data consist of broadband channels from stations with a worldwide distribution. In the initial phases of the project, approximately 15 stations were included; this number has now been increased to more than 100. The stations are equipped with a variety of instruments, including the broadband STS-2, CMG-3, and borehole KS-36000, and the very-broadband STS-1 and KS-54000 systems. We will see that the performance of the M_m algorithm is significantly affected by the nature of the recording system. Several stations were removed from the discussion, based on apparent inconsistencies in calibration or inadequate response at the lowest frequencies; the inadequate response could be caused by the choice of instrumentation, but also by site characteristics that can occasionally affect the performance of such instruments as the STS-2 seismometers.

The computation of M_m is activated manually by the operator on call and follows the algorithm described initially by Okal and Talandier (1989). This procedure deviates from the one used at CPPT and reflects both the greater number of detections of small events (which do not warrant the estimation of M_m) at PTWC, and the mandated presence, under PTWC operational standards, of an operator within minutes of a seismic detection (i.e., in many instances even before a distant event is properly located). Because of the abundance of stations reporting to PTWC, M_m estimates are limited to Rayleigh waves, because Okal and Talandier (1991) showed empirically and justified theoretically that the algorithm using Love waves could have a somewhat inferior performance. Another estimate of earthquake moment is also obtained at PTWC through the use of the so-called M_{wp} algorithm which computes the time integral of the ground displacement at teleseismic stations to recover the static value of M_0 as the integral of the moment rate function controlling the far-field body waves (Tsuboi *et al.*, 1995, 1999).

In operational mode, and for the purpose of the real-time assessment of the tsunami potential of a developing event, the maximum value of M_m at each station is retained, along the algorithm originally defined by Okal and Talandier (1989). However, the entire database of estimates of M_m at each individual period between 51 and 273 sec is archived into a permanent database. In comparison with real-time Centroid Moment Tensor (CMT) inversion algorithms, the information in the M_m database constitutes a different expression of essentially the same input data, but it is more complete because it is not restricted to the few frequencies targeted by the inversions, and it can thus provide a more detailed insight into source processes and questions relating to instrumentation response.

The estimated energy E^E radiated by the source is similarly computed on broadband records from stations located at an adequate distance from the source ($25° \leq \Delta \leq 90°$). We use the algorithm of Newman and Okal (1998) applied to a 70-sec time series, starting 5 sec before the predicted *P*-wave arrival time. Under operational conditions in real time, the value of Θ is obtained by using M_m to estimate the seismic moment:

$$\Theta = \log_{10} E^E - M_m - 20, \tag{5}$$

where E^E is in ergs. The calculation of Θ was implemented later than that of M_m in the evaluation algorithm at PTWC, and thus the size of the resulting dataset is smaller.

M_m Dataset

The M_m dataset consists of 119,643 measurements, taken at 14 periods on 8546 seismograms from 192 events recorded at 99 stations. Instrumentation was changed at Midway (MIDW), Wichita Mountains (WMOK), and Octopus Mountain (OCWA) during the course of the study; we then consider them as separate stations, bringing the total number of stations to 102. Note that the mere size of this dataset and its multidimensional character make it a challenge to evaluate the information that it contains. Figure 1 shows the geographical repartition of earthquakes and stations.

General Statistics for M_m

In this section, we discuss the performance of our M_m measurements against the values of the seismic moments M_0 eventually published in the Harvard CMT catalog (Dziewonski *et al.*, 2000, and subsequent quarterly updates). The latter are often interpreted in terms of a "moment magnitude,"

$$M_w = \frac{2}{3} [\log_{10} M_0 - 16.1], \tag{6}$$

where the factor 2/3 was introduced by Kanamori (1977) to mimic the behavior of M_s with M_0 in a range of moments where M_s undergoes partial saturation, and characteristic of many large, if not gigantic, earthquakes. To facilitate the interpretation of our results, we recast our measurements into the M_w scale, by defining $M_w(M_m) = 2/3\, M_m + 2.6$ and we focus on the residuals (defined as observed minus published values) $r_w = M_w(M_m) - M_w$. Note that these amount to 2/3 of the logarithmic residuals r on the estimate of the seismic moment, as defined by Okal and Talandier (1989).

We first consider the average value of the entire population of 119,643 residuals: $\overline{r_w} = -0.01$ units, and its standard deviation $\sigma_w = 0.27$. Although the former is excellent, the latter (equivalent to $\sigma = 0.41$) is significantly larger than reported in the early studies by Okal and Talandier (1989) or Hyvernaud *et al.* (1993). This is probably because of the full automation of the process, which can lead to the inclusion of spectral amplitudes close to noise level, stations at unfavorable distances, etc. Figure 2 further explores the variation of these parameters among individual stations, by plot-

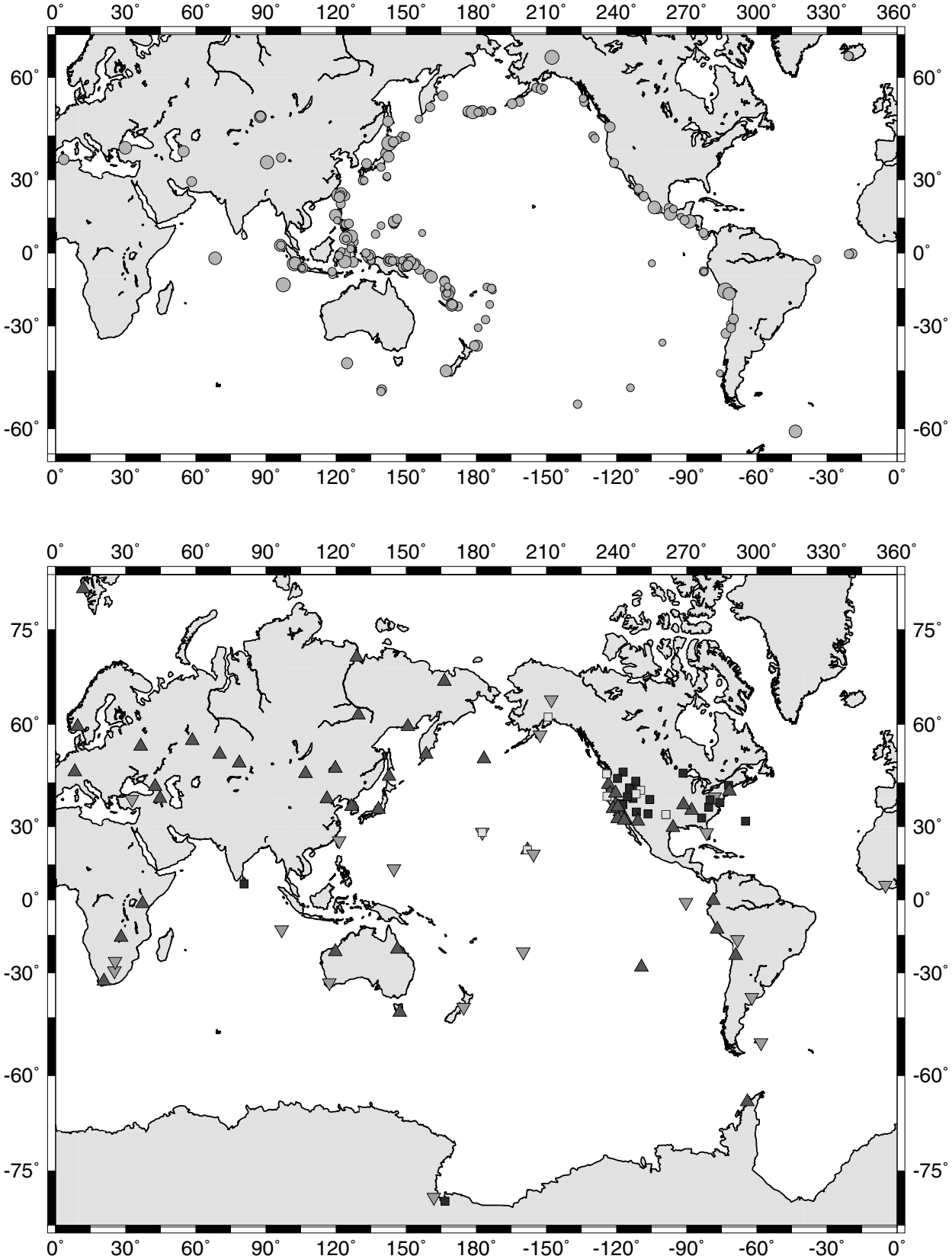

Figure 1. Maps of events (top) and stations (bottom) used in the M_m analysis. The size of the earthquake symbols expresses magnitude. Station symbols are upward-pointing triangles for STS-1 equipment, downward-pointing triangles for KS54000 equipment, open squares for STS-2 systems, and solid squares for "other" instruments.

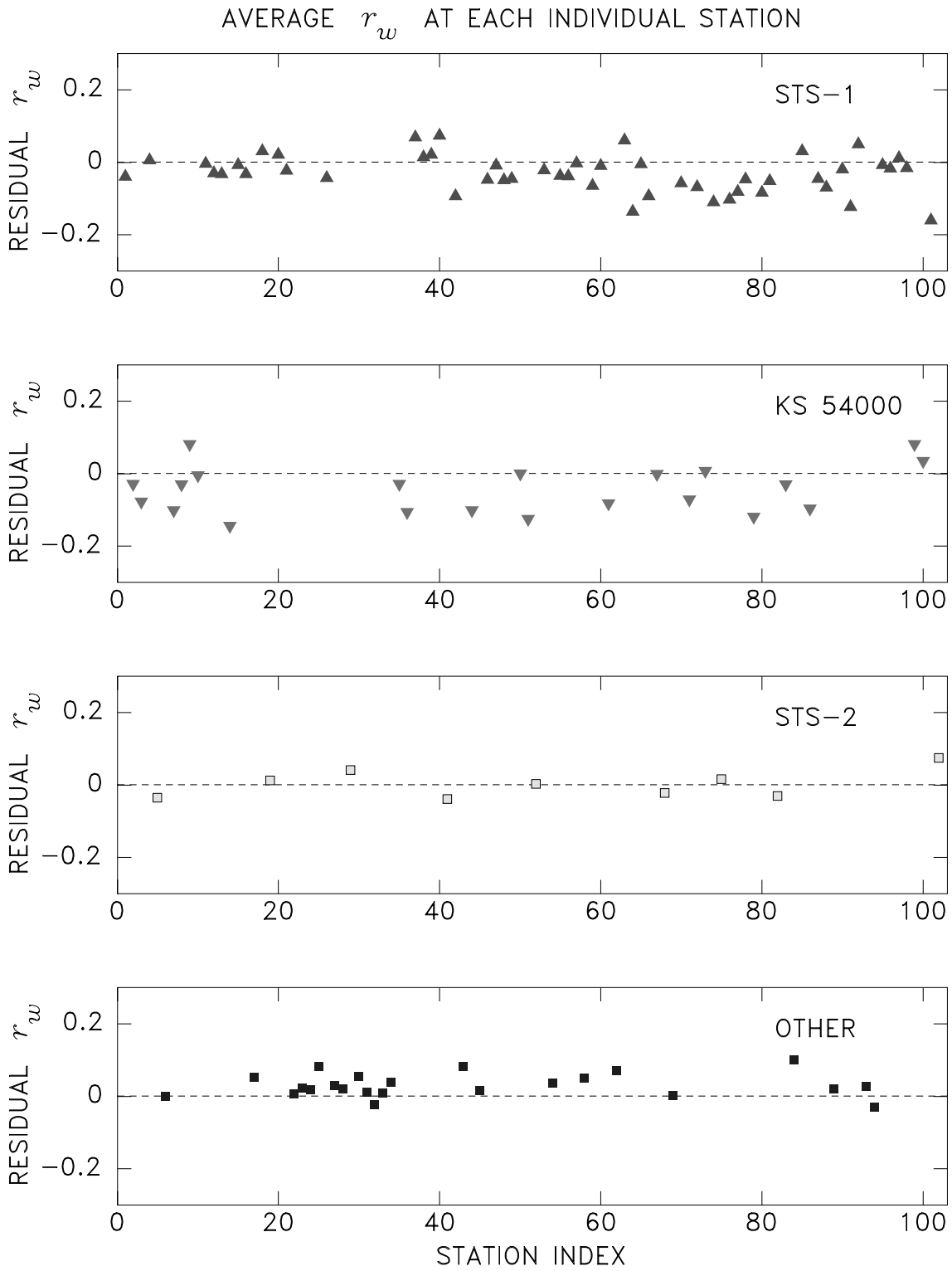

Figure 2. Average residual r_w observed at each station. Each symbol represents the average value of all residuals r_w computed at a particular station. The dataset has been partitioned (from top to bottom) between stations operating STS-1, KS-54000, STS-2, and "other" instruments. The station index used as the abscissa is arbitrary.

ting for each station the average of all residuals measured at that station. It is immediately clear that residuals at stations equipped with the very-broadband instruments, either STS-1 (49 stations) or KS54000 (21 stations) tend to be negative. Among non-very-broadband systems, the STS-2 instruments (nine stations) give average residuals of very low absolute value, whereas the remaining 23 stations (featuring instruments hereafter called "other") have more systematically positive average residuals. They are mostly equipped with CMG-3 sensors and overwhelmingly located in North America, as part of the U.S. National Seismic Network.

This trend is also expressed when the full population of measurements is split into just four subsets corresponding to the various instruments: we find $\overline{r_w} = -0.03$ for the STS-1 records (45% of the dataset), $\overline{r_w} = -0.05$ for the KS54000 ones (20%), $\overline{r_w} = +0.01$ for the STS-2 systems (10%), and $\overline{r_w} = +0.03$ for the "other" records (26%). Note that the STS-2 instruments perform better than the remainder of the non-very-broadband systems.

Next, we consider the influence of the spectral period T on the quality of the residuals. On Figure 3, we plot the average value of r_w for all measurements made at each of the 14 standard periods used between 51 and 273 sec. A significant increase in $\overline{r_w}$ is clearly detected for $T > 200$ sec ($f < 5$ mHz), with the final value ($T = 273$ sec) in excess of 0.15 unit. The bottom frames on Figure 3 and the full results listed in Table 1 show that, although this behavior is common for all types of instruments, it is moderate for the STS-1 and KS54000 systems, but stronger for the STS-2 instruments, and especially in the "other" records, where it reaches an average value of 0.28 units at $T = 273$ sec. Table 1 further shows that the variation with period of the performance of the STS-2 instruments is generally similar to that of the other non-very-broadband instruments: while residuals are excellent for $T \leq 150$ sec, they increase significantly at longer periods.

On Figure 4, we consider the residual r_w as a function of both the period T and the Harvard magnitude M_w of the event. Specifically, for each T, we bin the residual population into M_w intervals of 0.1 unit, and compute the average residual $\overline{r_w}$ in each bin. The five frames in the figure show the full dataset, the STS-1, KS54000, STS-2, and "other" subsets, respectively. They can be interpreted as a kind of report card for the various systems. The performance of the STS-1 instruments is remarkably stable with respect to frequency. Whereas the longest period ($T = 273$ sec) usually gives rise to the largest residuals, the difference is negligible, except for the smallest events ($M_w \leq 6.1$). The situation is very similar for the KS54000 instruments. For the combined STS-1 and KS54000 dataset, the scatter between measurements taken at the various periods has a standard deviation σ_w of less than 0.1 units across the magnitude range. By contrast, the "other" instruments show a systematic scatter reaching 0.15 unit, the residuals at 273 sec being systematically 0.25 or more units above those at other periods. The situation is clearly exacerbated for the smaller events, for which the residual r_w at the longest period can reach 0.6 unit, or a full order of magnitude in the moment M_0. This is explained simply as a combination of the reduced generation of very-long-period energy by the smallest events and of the poorer response of these instruments, as compared with the superior very-broad-band STS-1 and KS54000 systems. As a result, for the longest periods and the smallest events, the STS-2 and "other" instruments may not be recording above noise level.

We conclude that the performance of the KS54000 system is comparable with that of the STS-1 instrument across the frequency band, but that measurements on STS-2 and "other" systems should not be included at periods longer than 205 and 140 sec, respectively. In addition, we verified that the five stations operating the KS36000 system (included in the "other" instruments) had a performance comparable with those equipped with the KS54000 system.

Retaining Maximum M_m for Each Record

Under the operational motivation of having to derive in real time the true size and tsunamigenic potential of a distant earthquake, we consider a number of strategies to condense, for each earthquake, a large set of measurements (which now routinely reaches 1000 M_m values) into the best possible estimate of a seismic moment.

In Table 2, we first study the performance of the operational procedure defined and used by Okal and Talandier (1989) under which, for each record, one retains the largest value of M_m over the various frequencies considered in the spectral domain. The rationale behind this approach is that interference effects caused by source finiteness are expected to be destructive, and thus the largest value of M_m should be the least affected and most representative of the true size of the earthquake (Okal and Talandier, 1989). Using this algorithm, we find an average residual $\overline{r_w} = 0.25$ unit, with $\sigma_w = 0.25$ for the entire dataset of 8546 records, $\overline{r_w} = 0.19$ for the STS-1 records, $\overline{r_w} = 0.20$ for the KS54000 records, but $\overline{r_w} = 0.31$ for the STS-2 records, and $\overline{r_w} = 0.35$ for the "other" instruments.

For each earthquake, we then proceed to average these individual maximum M_m values over all stations contributing data. Figure 5 shows the resulting event-averaged residual, as a function of the Harvard CMT moment, expressed as a magnitude M_w. The residuals are systematically positive and tend to decrease with increasing moment, the trend being strongest for the STS-2 and "other" instruments. We note on Figure 6 that an overwhelming majority of the maximum magnitudes are retained at the longest period, $T = 273$ sec; however, the origin of this trend is instrument dependent, because the performance of the "other" types is strongly degraded at that period. In this respect, we examine in Table 2 the influence of excluding $T = 273$ sec and retaining, again for each record, the maximum M_m among the remaining periods. We find that the performance of this new algorithm is expectedly improved, especially for the STS-2

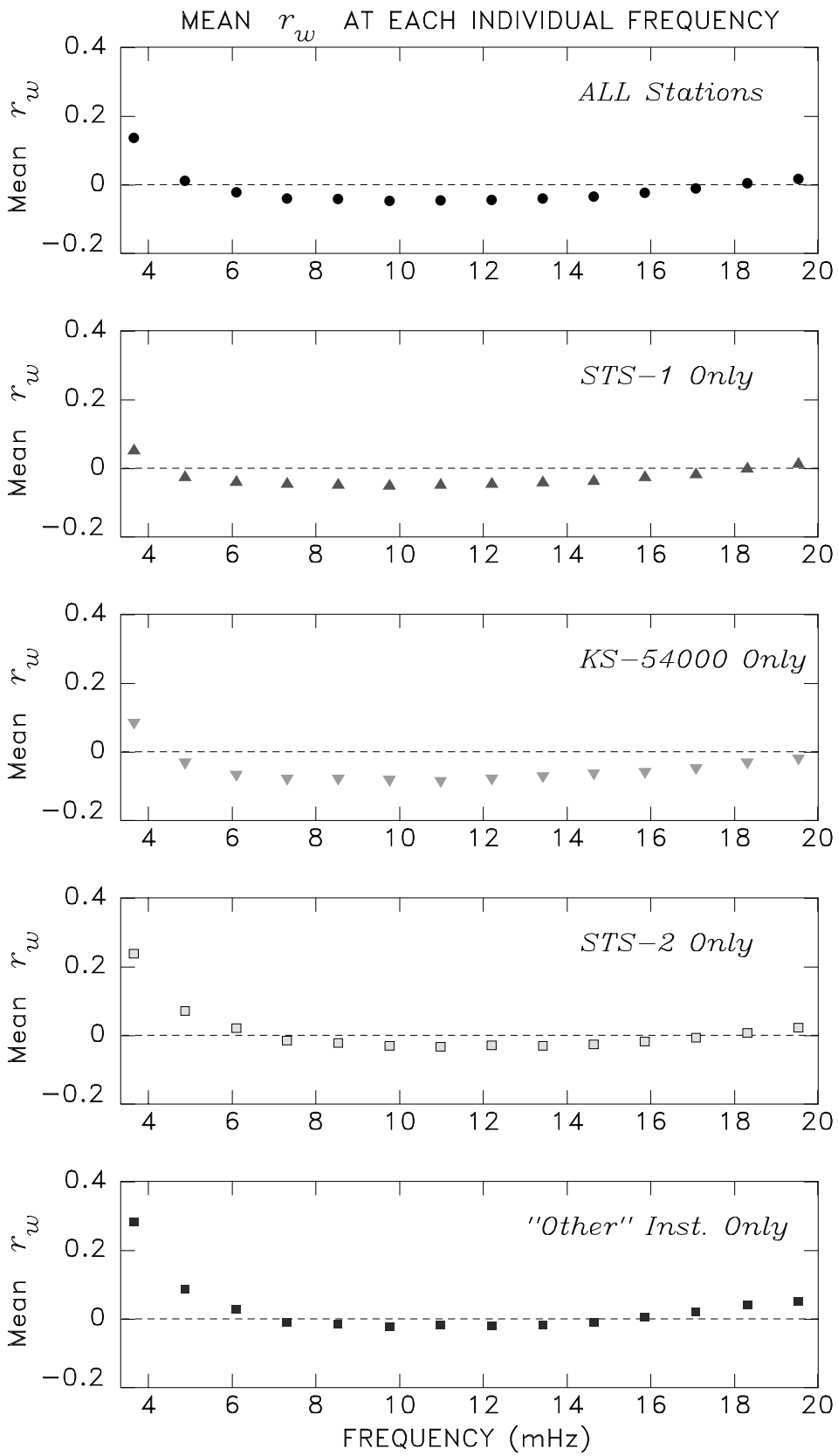

Figure 3. Frequency dependence of the residuals r_w. On the top frame, we plot for each of the 14 standard frequencies considered between 3.7 and 19.5 mHz ($51 \leq T \leq 273$ sec), the average value of all residuals r_w measured at that frequency. The four lower frames further split this dataset according to the type of instrument used.

Table 1
Residual Statistics of the Full M_m Dataset

T (sec)	Full Dataset (8546 Records)		STS-1 Only (3822 Records)		KS54000 Only (1676 Records)		STS-1 and KS54000 (5498 Records)		STS-2 Only (867 Records)		"Other" Instruments (2181 Records)	
	r_w	σ_w	r_w	σ_w	r_w	σ_w	r_w	σ_w	r_w	σ_w	r_w	σ_w
All Periods												
	0.01	0.27	−0.03	0.26	−0.05	0.27	−0.03	0.27	0.01	0.28	0.03	0.28
Break According to Period												
51	0.02	0.26	0.01	0.26	−0.02	0.27	0.00	0.27	0.02	0.26	0.05	0.25
55	0.00	0.26	0.00	0.26	−0.03	0.26	−0.01	0.26	0.01	0.25	0.04	0.25
59	−0.01	0.26	−0.02	0.26	−0.05	0.26	−0.03	0.26	−0.01	0.26	0.02	0.24
63	−0.02	0.26	−0.03	0.26	−0.06	0.26	−0.04	0.26	−0.02	0.26	0.01	0.25
68	−0.03	0.26	−0.04	0.26	−0.06	0.25	−0.05	0.25	−0.03	0.26	−0.01	0.25
74	−0.04	0.26	−0.04	0.25	−0.07	0.26	−0.05	0.26	−0.03	0.26	−0.02	0.26
82	−0.04	0.25	−0.05	0.25	−0.08	0.26	−0.05	0.25	−0.03	0.25	−0.02	0.25
91	−0.05	0.26	−0.05	0.25	−0.08	0.26	−0.06	0.26	−0.03	0.26	−0.02	0.25
102	−0.05	0.26	−0.05	0.25	−0.08	0.26	−0.06	0.26	−0.03	0.26	−0.02	0.26
117	−0.04	0.27	−0.05	0.26	−0.08	0.27	−0.06	0.26	−0.02	0.27	−0.01	0.27
137	−0.04	0.27	−0.05	0.27	−0.08	0.27	−0.05	0.27	−0.01	0.28	−0.01	0.27
164	−0.02	0.28	−0.04	0.27	−0.07	0.28	−0.05	0.27	0.02	0.28	0.03	0.27
205	0.01	0.29	−0.03	0.27	−0.03	0.29	−0.03	0.28	0.07	0.31	0.09	0.30
273	0.14	0.32	0.05	0.28	0.09	0.30	0.06	0.29	0.24	0.33	0.28	0.32

and "other" instruments, whose average residual nevertheless remains high. Most significantly, the performance of the STS-1 remains consistent across the whole magnitude range (mean residual $\overline{r_w} = 0.15 \pm 0.20$ unit; mean event-averaged 0.14 ± 0.13 unit). The trend of r_w with increasing M_w decreases significantly (from a slope of -0.20 to -0.13) for the STS-2 and "other" instruments, which confirms that the numerous instances of maximum M_m at 273 sec may be attributable to poor response in those instruments (and especially for small earthquakes; see Fig. 4). The decrease is less important (from a slope of -0.14 to -0.12) for very-broadband systems featuring a superior response; this expresses the enhanced reliability of the M_m scale toward long periods at which interference effects are expected to be minimized, which indeed motivated the development of M_m by Okal and Talandier (1989).

We explored the possibility of further improving the performance of the algorithm by restricting the range of allowable periods to $70 \leq T \leq 250$ sec. This has the effect of eliminating the highest frequencies, at which exact source depth and lateral heterogeneities can have a detectable effect on the spectral amplitudes of mantle waves (Okal and Talandier, 1989). The average residuals for the STS-1 and KS54000 systems are decreased significantly to a mean residual of 0.09 unit and a mean event-averaged residual of 0.08 unit. The trend of r_w with moment is not changed significantly. Some improvement is also achieved for the STS-2 and "other" instruments, but their performance still trails that of the very-broadband systems.

In conclusion, an algorithm based on retaining the maximum value of M_m for each record can provide mean and mean event-averaged residuals of less than 0.1 unit, as long as the method is restricted to the superior STS-1 and KS54000 systems and to the period range 70–250 sec (in practice, 74–205 sec). Under these conditions, the performance of the STS-1 and KS54000 systems is essentially equivalent.

Averaging All Values of M_m for Each Record

Another approach consists of averaging over period the values of M_m for each record, rather than retaining the largest one. Because the number of periods at which individual measurements are taken is essentially constant, the mean $\overline{r_w}$ of these populations of residuals would be equivalent to those present in the first line of Table 1; their σ_w would, however, be lower.

Once again, we then define, for each event, a mean residual by averaging the previous values over the reporting stations, and we thus obtain a new estimate of the moment of the earthquake. The resulting residuals are presented on Figure 7 as a function of published (Harvard) M_w, and their statistics are listed in Table 3. As expected, we find lower residuals than when using a maximum M_m. Both the STS-1 and KS54000 values become, on the average, slightly negative ($\overline{r_w} = -0.04$ and -0.06, respectively), but their scatter, typically 0.14 units, remains comparable with that of the previous algorithm. As for the STS-2 and "other" instruments, this procedure is the only one significantly improving the mean and standard deviation of their residuals to values comparable with those of the very-broadband instruments; once again, the behavior of the STS-2 systems is similar to that of the whole "other" dataset. As a result, the full dataset also features much improved residuals.

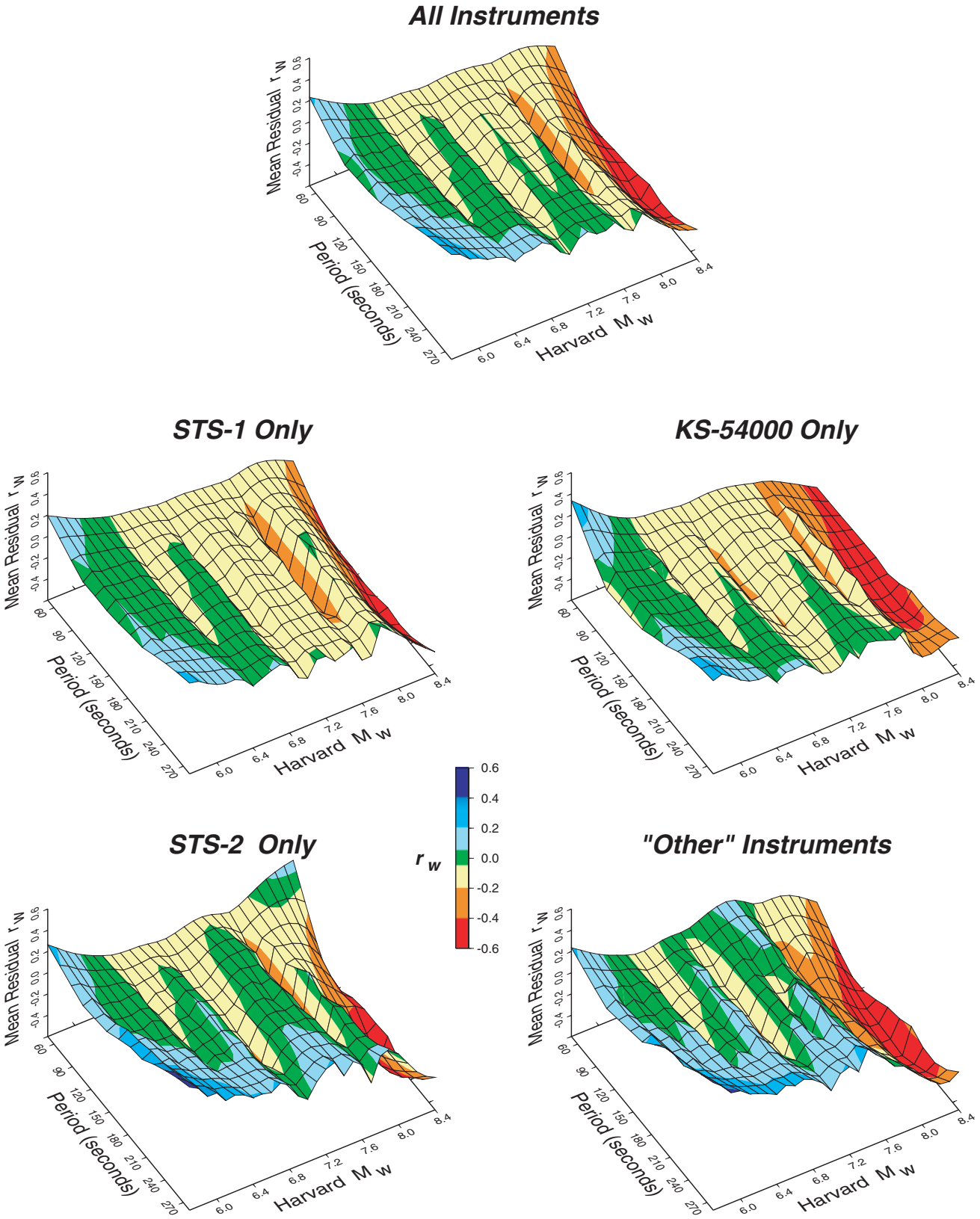

Figure 4. Three-dimensional plots of the residuals r_w as a function of period and seismic moment (expressed as M_w published in the Harvard catalog). For each of the standard frequencies, values of r_w are regrouped in magnitude bins of width 0.1 M_w-unit, and an average value computed in each bin. The resulting function is then plotted in three dimensions and color coded. Separate plots are made for the various types of instruments.

Table 2
Residual Statistics Using the Maximum Value of M_m for Each Record

	Full Dataset (8546 Records)		STS-1 Only (3822 Records)		KS54000 Only (1676 Records)		STS-1 and KS54000 (5498 Records)		STS-2 Only (867 Records)		"Other" Instruments (2181 Records)	
	r_w	σ_w	r_w	σ_w	r_w	σ_w	r_w	σ_w	r_w	σ_w	r_w	σ_w
Retain maximum M_m for each record												
Mean residual	0.25	0.25	0.19	0.22	0.20	0.23	0.19	0.22	0.31	0.29	0.35	0.26
Mean event-averaged	0.24	0.13	0.17	0.13	0.19	0.13	0.18	0.12	0.31	0.19	0.35	0.17
Retain maximum M_m (excluding $T = 273$ sec)												
Mean residual	0.18	0.22	0.15	0.20	0.14	0.21	0.15	0.21	0.21	0.24	0.24	0.22
Mean event-averaged	0.17	0.12	0.14	0.13	0.14	0.12	0.14	0.12	0.21	0.17	0.23	0.16
Retain maximum M_m (only $70 < T < 250$ sec)												
Mean residual	0.12	0.23	0.09	0.21	0.08	0.22	0.09	0.21	0.16	0.25	0.18	0.24
Mean event-averaged	0.11	0.13	0.08	0.13	0.08	0.12	0.08	0.12	0.16	0.18	0.18	0.17

Guided by our experience with the previous approach, we also explored the influence of a reduction in the period range over which M_m values are retained, by imposing $T > 70$ sec, and also $T < 165$ sec for the non-very-broadband instruments. As detailed in Table 3, this leaves the population of very-broadband residuals r_w essentially unchanged, but improves the "other" dataset.

A final combination of these various approaches consists, for every event, of focusing on each of the standard M_m periods and, at each of them, of averaging the individual measurements at all stations (although we eliminate STS-2 records for $T > 205$ sec, and the "other" instruments for $T > 137$ sec). For each event, we then retain as a measure of the moment, the maximum among the various averages thus obtained at each period. The resulting population of residuals is shown on Figure 8, as a function of published Harvard M_w, and features a mean value $\overline{r_w} = -0.10$ and a standard deviation $\sigma_w = 0.12$ units.

The Case of the Largest Events: Peru 2001 and Hokkaido 2003

We now address in detail the question of the performance of the various algorithms for the largest earthquakes in the dataset, specifically the Peruvian earthquake of 23 June 2001 ($M_0 = 4.7 \times 10^{28}$ dyne cm), and the Hokkaido earthquake of 25 September 2003 ($M_0 = 3.05 \times 10^{28}$ dyne cm), at the time the largest and third largest events in the Harvard CMT catalog. As evidenced on Figures 5 and 7, these earthquakes have systematically large, negative residuals. It is important to understand the origin of this problem, because it is in strong contrast with the original studies by Okal and Talandier (1989, 1990, 1991), which had developed the M_m algorithm precisely to obtain an accurate estimate of the largest earthquakes, and validated its use even on the gigantic Chilean and Alaskan earthquakes of 1960 and 1964.

Peru, 23 June 2001. The 2001 Peruvian earthquake contributed 40 stations to the PTWC dataset, for a total of 560 M_m measurements. The average residual is a very disappointing $\overline{r_w} = -0.51$ units, with $\sigma_w = 0.19$. Significantly, the residuals are poor for all types of instruments ($\overline{r_w} = -0.54$, -0.47, -0.47, and -0.49 for STS-1, KS54000, STS-2, and "other" systems, respectively).

As summarized by Okal *et al.* (2002), the early estimates of the moment of the 2001 Peruvian earthquake were significantly scattered. The Harvard "QUICK" solution proposed $M_0 = 1.23 \times 10^{28}$ dyne cm, Kikuchi and Yamanaka (2001) proposed $M_0 = 2.2 \times 10^{28}$ dyne cm, and the National Earthquake Information Center proposed $M_0 = 3.7 \times 10^{28}$ dyne cm. These values were significantly lower than the final Harvard solution and would correspond to r_w residuals of -0.39, -0.22, and -0.07, respectively. By contrast, the estimate from Papeete ($M_0 = 4.9 \times 10^{28}$ dyne cm) was in excellent agreement with the final moment ($r_w = 0.01$).

In seeking an explanation to this pattern, we note on Figure 9 that all but nine stations in our dataset are at an azimuth of $330° \pm 27°$ from the epicenter, that is, only 20° from the strike of the fault plane. In addition, several source studies have shown that the rupture propagated in the opposite direction, that is, east-southeast over at least 140 km, and possibly 250 km (Kikuchi and Yamanaka, 2001; Bilek and Ruff, 2002). Thus, the bulk of the stations suffer from the combination of an unfavorable radiation pattern and a severe directivity effect. We verified this interpretation by correcting our estimates of M_m for focal mechanism (along the lines of "M_c" as described by Okal and Talandier [1989]), and directivity, using the longer fault (250 km) and a rupture velocity of 3 km/sec. We restrict this computation to the longest periods ($T > 200$ sec), because the shorter ones would be significantly affected by the details of the presumably inhomogeneous rupture. The average residual then falls to $\overline{r_w} = -0.08$, an acceptable value.

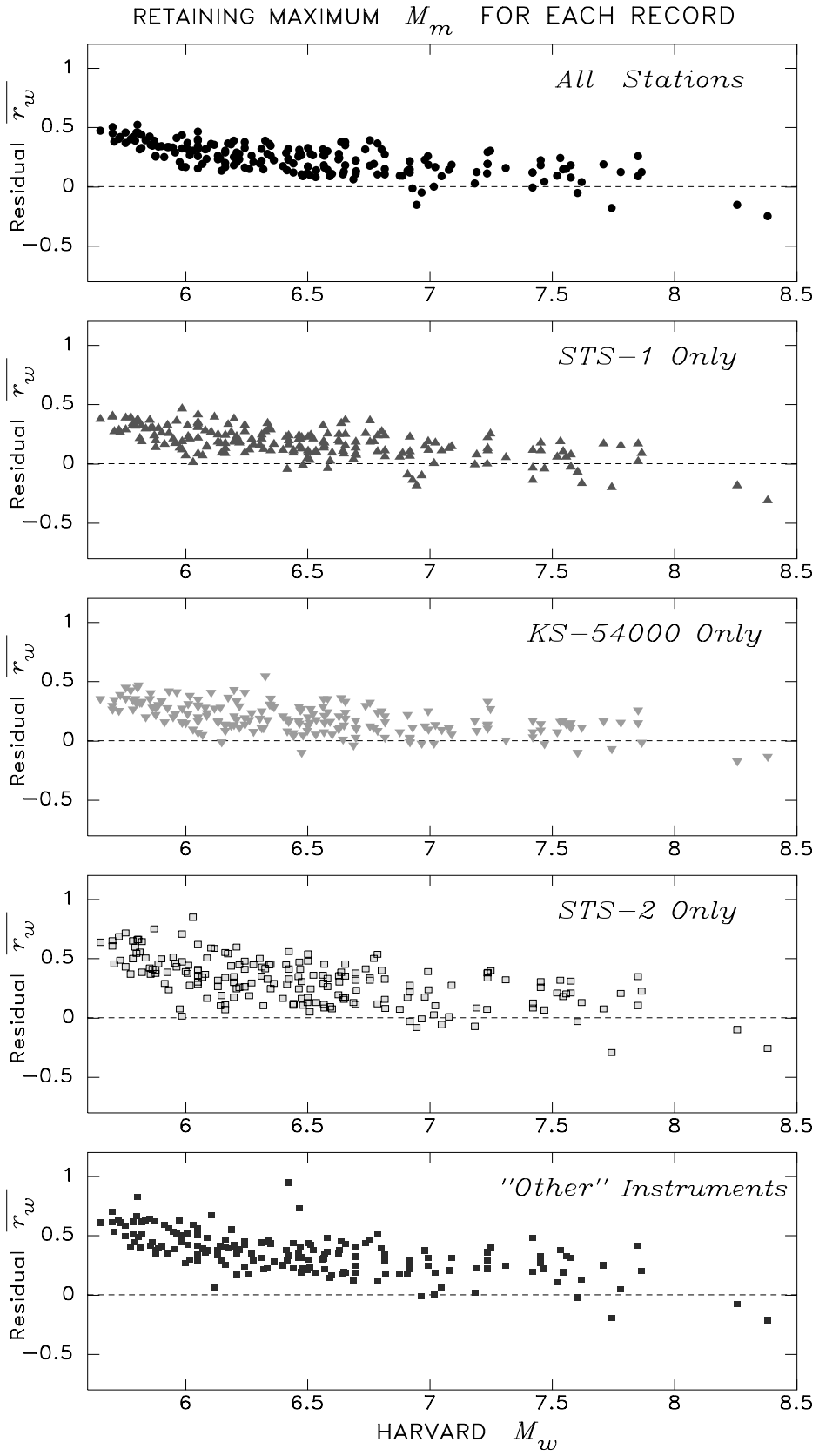

Figure 5. Performance of the algorithm retaining, for each record, the maximum value of M_m across the frequency spectrum. For each earthquake, these maximum M_m values are then averaged over all reporting stations. The resulting $\overline{r_w}$ is then plotted against the published [Harvard] M_w. Note the excellent performance of the STS-1 and KS54000 systems, the latter even for the largest earthquakes, but the larger residuals obtained at small magnitudes on the STS-2 and "other" instruments.

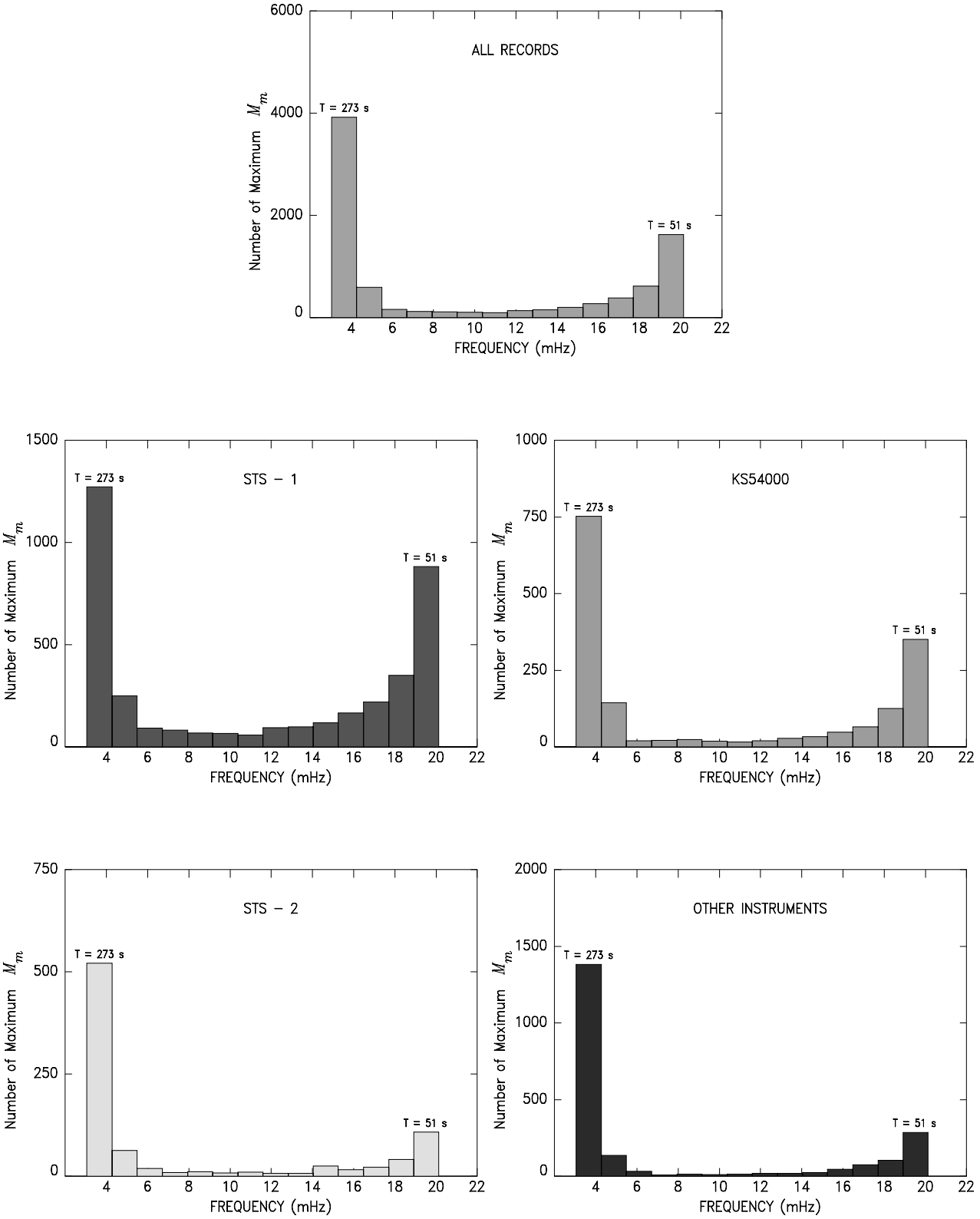

Figure 6. Histograms of the numbers of measurements of maximum M_{m} made at each of the reference frequencies. Note the preponderance of measurements made at the longest period ($T = 273$ sec), especially for the "other" instruments.

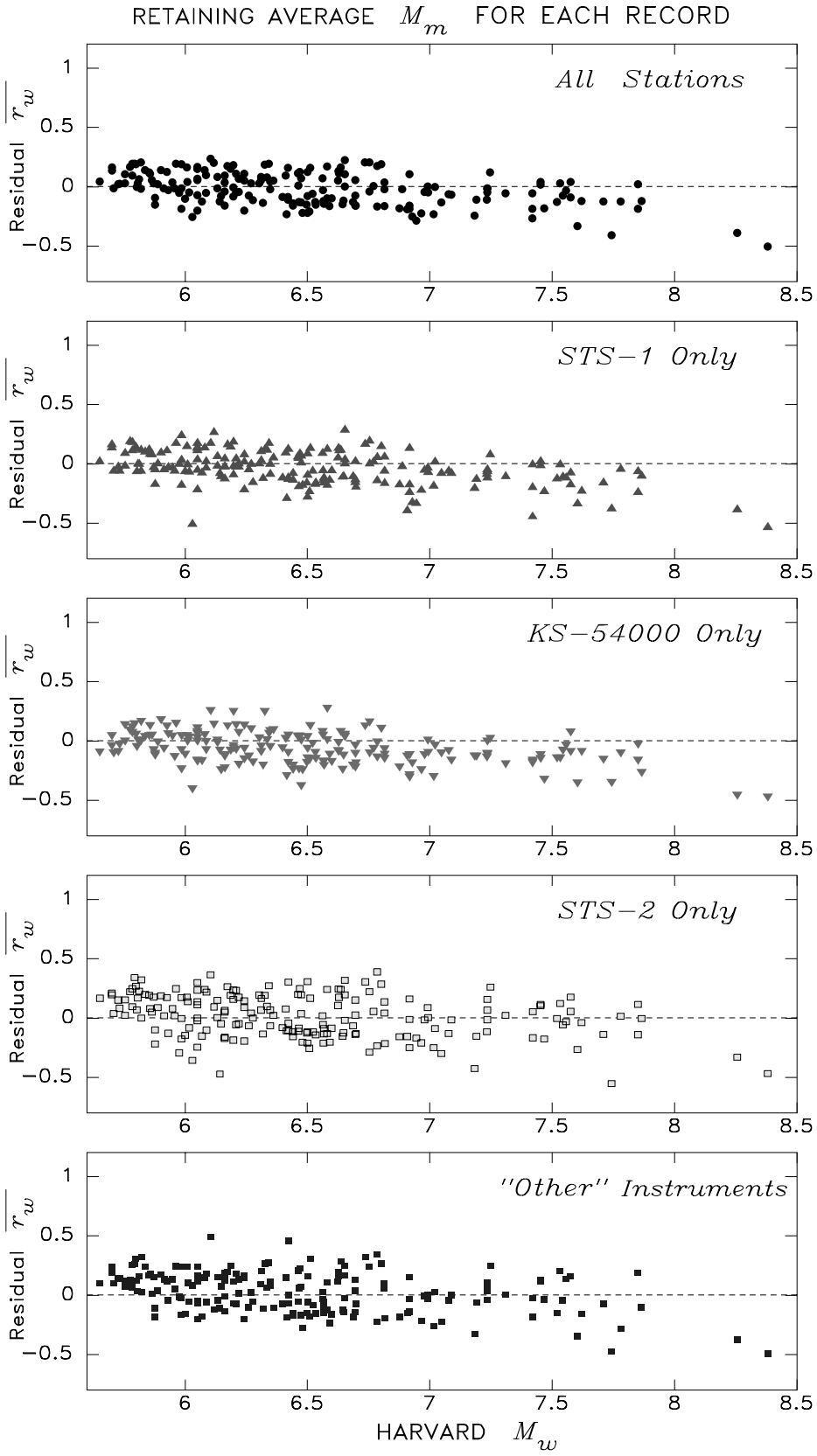

Figure 7. Same as Figure 5, using for each record the average values of M_m computed at all sampled frequencies. $\overline{r_w}$ is the mean residual obtained for each earthquake by averaging such values over all contributing stations.

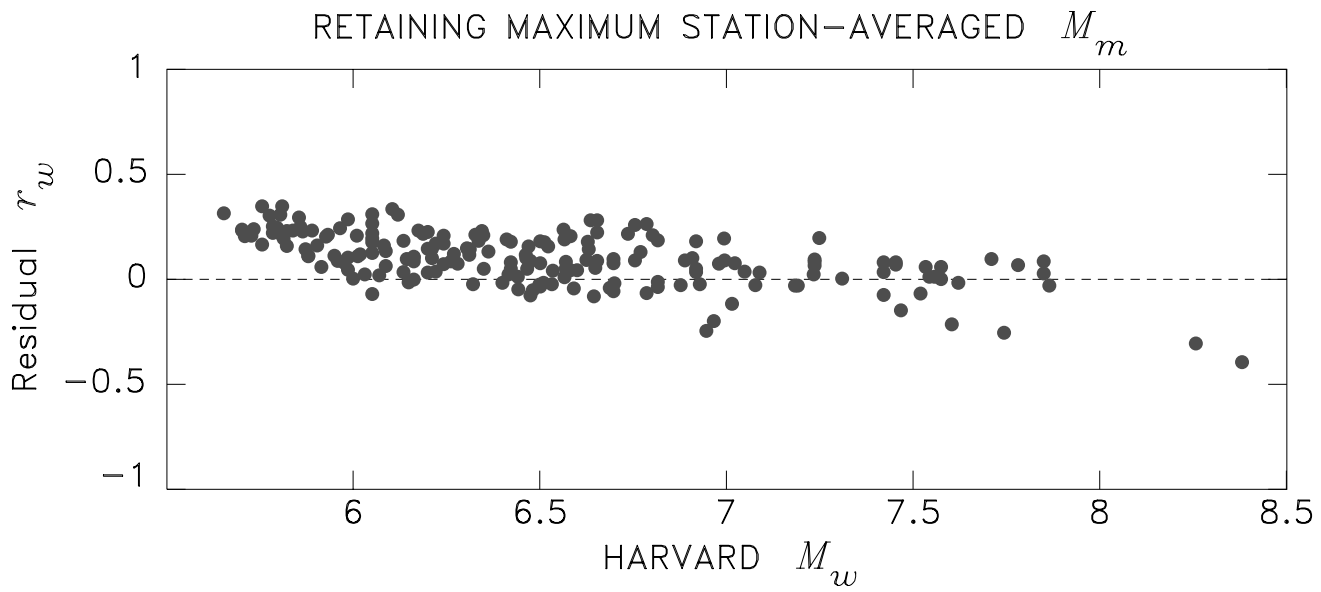

Figure 8. Population of residuals r_w obtained by first averaging M_m values at each period over all contributing stations (with some limitations on non-very-broadband instruments; see text for details), and then retaining the maximum value of the resulting averages over the full period range. Residuals are given against CMT moment values published by Harvard.

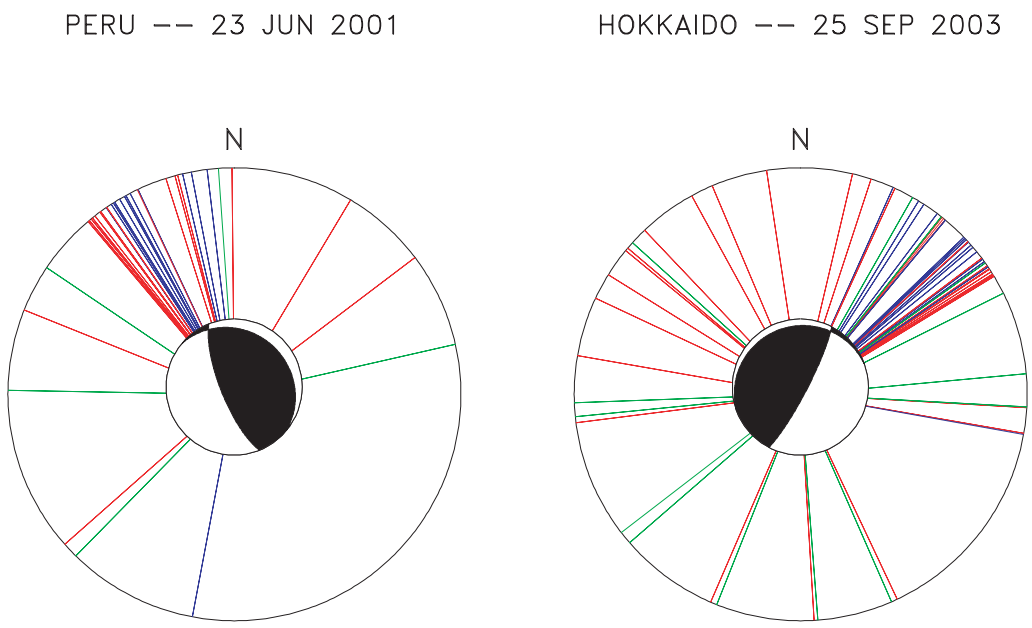

Figure 9. Azimuthal distributions of stations contributing M_m measurements for the 2001 Peruvian earthquake (left) and the 2003 Hokkaido event (right). Each individual radius represents one station, color-coded by instrument (STS-1, red; KS54000, green; STS-2 and "other," blue). The focal mechanisms of the events are shown for reference at the center of each diagram.

Hokkaido, 25 September 2003. The 2003 Tokachi-Oki earthquake in Hokkaido, Japan, contributed 840 M_m values from 60 stations, with $\overline{r_w} = -0.39$ and $\sigma_w = 0.24$. Results are similarly mediocre for all classes of instruments ($\overline{r_w} = -0.38$, -0.45, -0.33, and -0.37, respectively, for STS-1, KS54000, STS-2, and "other" systems). Although the azimuthal repartition of the stations is slightly more regular than for the 2001 Peru event, there is still a strong clustering of mostly North American stations in the azimuth of the fault plane (Fig. 9). Correcting M_m values for focal mechanism

and directivity, based on preliminary estimates of a 200-km rupture directed east-northeast (Kasahara *et al.*, 2003), results in $\overline{r_w} = -0.12$, a much more acceptable value, for the 120 measurements with $T > 200$ sec.

The Slowness Parameter Θ

Our dataset comprises 3192 values of Θ obtained from 118 earthquakes recorded at 122 stations. It is presented on Figure 10 as a function of epicentral distance. The mean value, $\bar{\Theta} = -5.12$, and the standard deviation, $\sigma_\Theta = 0.58$, are comparable with those obtained by Newman and Okal (1998) in their initial analysis (-5.02 ± 0.61). The low correlation coefficient of Θ with distance (-0.16) confirms the adequate character of the algorithm's distance correction. Figure 11a plots the same dataset as a function of published Harvard M_w and Figure 11b presents the results of averaging, for each event, over all contributing stations. This latter dataset of 118 values has an average $\bar{\Theta}$ of -5.10, with $\sigma_\Theta = 0.39$, once again in excellent agreement with the corresponding values in Newman and Okal's (1998) study (-5.06 ± 0.46). The datasets are also presented as histograms on Figure 12. Note that the distribution of event-averaged Θ is peaked precisely at the theoretical value (-4.90) expected from scaling laws (Newman and Okal, 1998).

On Figure 13, we combine our dataset with that of Newman and Okal (1998) and map the resulting 190 epicenters, color-coded according to Θ. We clearly fail to reveal a regional trend in the values of Θ, a conclusion already reached in Central America, Peru, and the Sunda Arc by Okal and Newman (2001). However, Figures 11b and 13 readily identify (by Julian date) several events featuring anomalously low values of Θ, and thus deserving further discussion.

The 2001 Peruvian Earthquake

Once again we find an anomalous result for this event, namely that its estimated energy, and hence Θ, are significantly underestimated by our algorithm ($\Theta = -6.53$). This contradicts its large value of m_b (6.7), high intensities and resulting extensive and widespread damage in the epicentral area, and indeed the substantially larger value of Θ (-5.48) reported by Okal *et al.* (2002). We can trace the origin of that discrepancy to these authors' slightly different algorithm, which utilized a longer time window (100 sec).

To investigate this problem in more detail, we study in Figure 14 the influence on the final value of Θ of delaying the time window used for the computation of the estimated energy E^E. A 70-sec window is moved in 10-sec steps from a zero delay (i.e., the window starting 5 sec before the theoretical *P* arrival), to a full 100-sec delay. We interpret our results, shown in frame a, as indicating that the main energy in the *P* wave train emerges only about 60 sec into the signal. This is in general agreement with several source tomography studies (Bilek and Ruff, 2002; Giovanni *et al.*, 2002), which have identified two pulses in the time function, the second one delayed 70 sec and contributing most of the moment release, the earthquake being in a sense "late." Thus, the standard algorithm using the first 70 sec of signal misses the main pulse and yields an artificially deficient Θ. As the window is moved up in time, the algorithm catches the main moment release and Θ reverts back to a value (-5.65) more in line with the results of Okal *et al.* (2002) (-5.48).

By contrast, we consider in Figure 14b two "regular" earthquakes, namely the main Peruvian aftershock of 7 July 2001 ($M_0 = 3.2 \times 10^{27}$ dyne cm) and the 2003 Tokachi-Oki earthquake discussed in the M_m Dataset section. In both

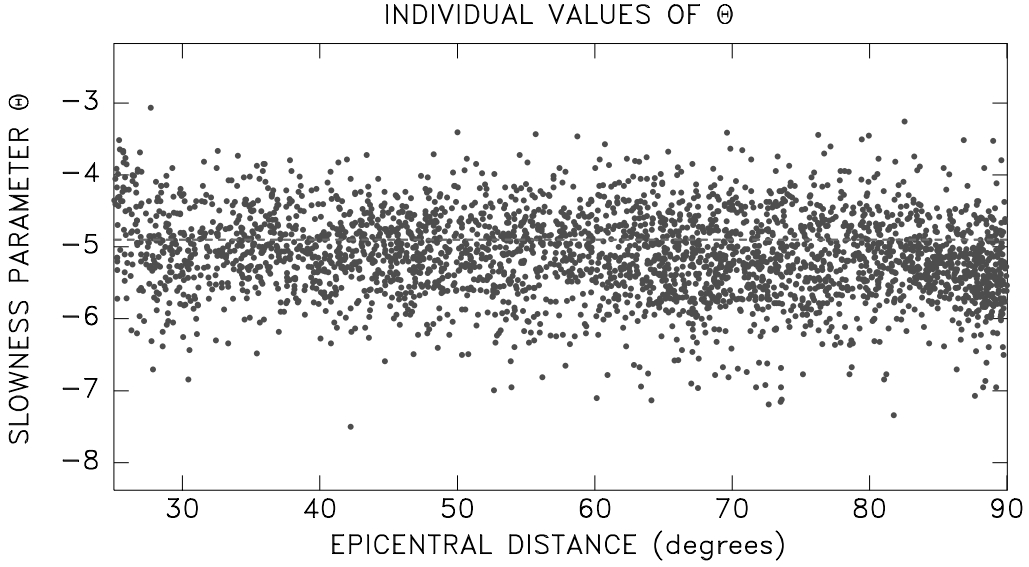

Figure 10. Values of Θ measured on 3192 records at individual stations plotted as a function of epicentral distance. The dashed line is the theoretical value (-4.90) predicted by scaling laws.

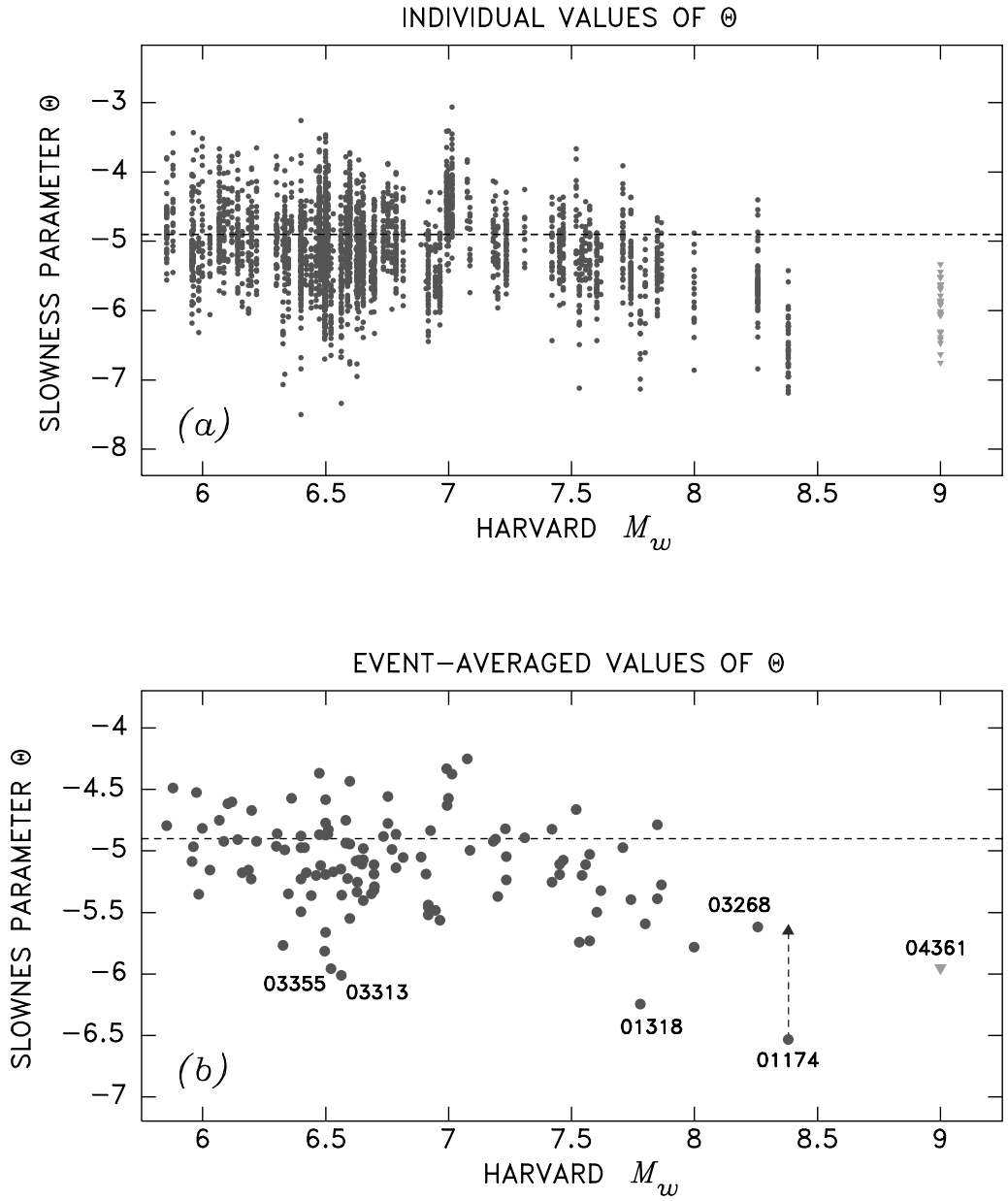

Figure 11. Slowness parameter Θ plotted as a function of Harvard magnitude M_w. (a) Individual values from 3192 records. (b) Event-averaged values. Events identified by Julian date (including those featuring deficient Θ) are discussed in the text. The vertical dashed segment and upward-pointing triangle show the corrected value of Θ for the 2001 Peruvian mainshock, obtained by using a sliding time window. On both frames, the horizontal dashed line shows the theoretical value (−4.90) predicted by scaling laws. In addition, and on both frames, the inverted triangles refer to a preliminary analysis of the 2004 Sumatra earthquake (see Appendix).

cases, we see a decrease in Θ with increased window delay. For the smaller event, the estimated energy is adequately evaluated and a representative value of Θ obtained (in this case, −5.5, moderately slow) for the first three steps, but later values become strongly deficient (Θ = −6.0 to −6.3), as the window simply no longer samples the *P* wave. This interpretation suggests that the duration of the *P*-wave signal is about 25 sec, in excellent agreement with the total duration inverted by Giovanni *et al.* (2002). For the Hokkaido event, the situation is essentially similar, except that its larger size results in a longer source duration, observed at about 60 sec.

We also examine on Figure 14c the three classic "tsunami earthquakes" of the past decade (Nicaragua, 1992; Java, 1994; and Chimbote, Peru, 1996), using the original records from Newman and Okal's (1998) study. These three earthquakes are characterized by a very slow but relatively

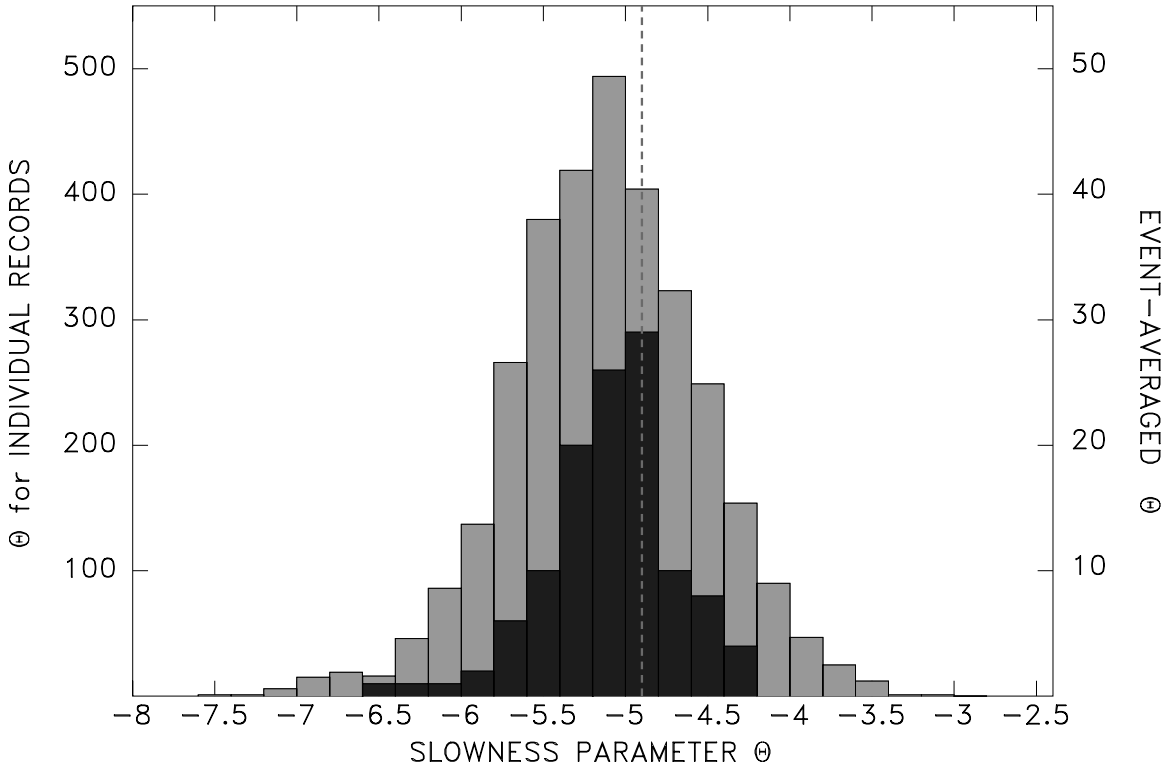

Figure 12. Distribution of Θ values obtained in this study, binned in intervals of 0.2 logarithmic units. The background light-colored histogram refers to individual records (left vertical scale), the darker one refers to event-averaged values (right vertical scale). The vertical dashed line ($\Theta = -4.90$) is the theoretical value predicted by scaling laws.

continuous rupture, which results in a low value of Θ, essentially independent of the time window considered. This pattern is fundamentally different from that of the 2001 Peru mainshock, which is not intrinsically ultraslow but rather features a small precursor, followed by a main pulse, both of them exhibiting no more than a trend toward slowness. The three "tsunami earthquakes" are slow events; the 2001 Peruvian shock is merely "late."

Finally, on Figure 14d, we consider the three strike-slip events featuring low values of Θ, namely the Kunlun, Tibet, earthquake of 14 November 2001, and two recent events on the Mid-Atlantic Ridge. In the Kunlun event, the deficiency in Θ expresses the very-low-stress drop documented by Lin *et al.* (2003) even though Bouchon and Vallée (2003) have argued that the rupture was fast, actually "supershear." The low-stress drop could be attributed to decoupling of the fault walls through the presence of a zone of weak fault gauge as surveyed by Wang *et al.* (2003). We find remarkably similar results in the two Mid-Atlantic Ridge earthquakes of 9 November and 21 December 2003, which both feature a very stable and highly deficient value of Θ (-6.01 and -5.96, respectively). This property does not simply reflect a bias introduced into E^E by the strike-slip geometry of faulting, because previous studies (e.g., Okal and Stewart, 1982; Stewart and Okal, 1983) have evidenced a high degree of diversity in seismic coupling along midoceanic transform faults, with Okal and Langenhorst (2000) documenting a regular population of Θ values (with an average value of -4.90) on the Eltanin system. In this respect, our results concerning the two Mid-Atlantic Ridge events would suggest an anomalous morphology of the relevant transform faults.

Discussion and Conclusion

Our experience during five years of routine application of the M_m algorithm at PTWC confirms that it can provide accurate real-time estimates of the seismic moment of major teleseismic events. The best results are clearly obtained by restricting the computation to those stations equipped with very-broadband instruments. In this respect, the performance of the two systems (STS-1 and KS54000) is equivalent. Results from the few available STS-2 instruments are not markedly different from those of the other non-very-broadband systems.

Okal and Talandier's (1989) original algorithm, which consists of retaining for each record the maximum value computed for M_m, then yields acceptable residuals r_w (on the average less than 0.1 unit) in the frequency range 4–14 mHz (70–250 sec), with the inclusion of the very longest period

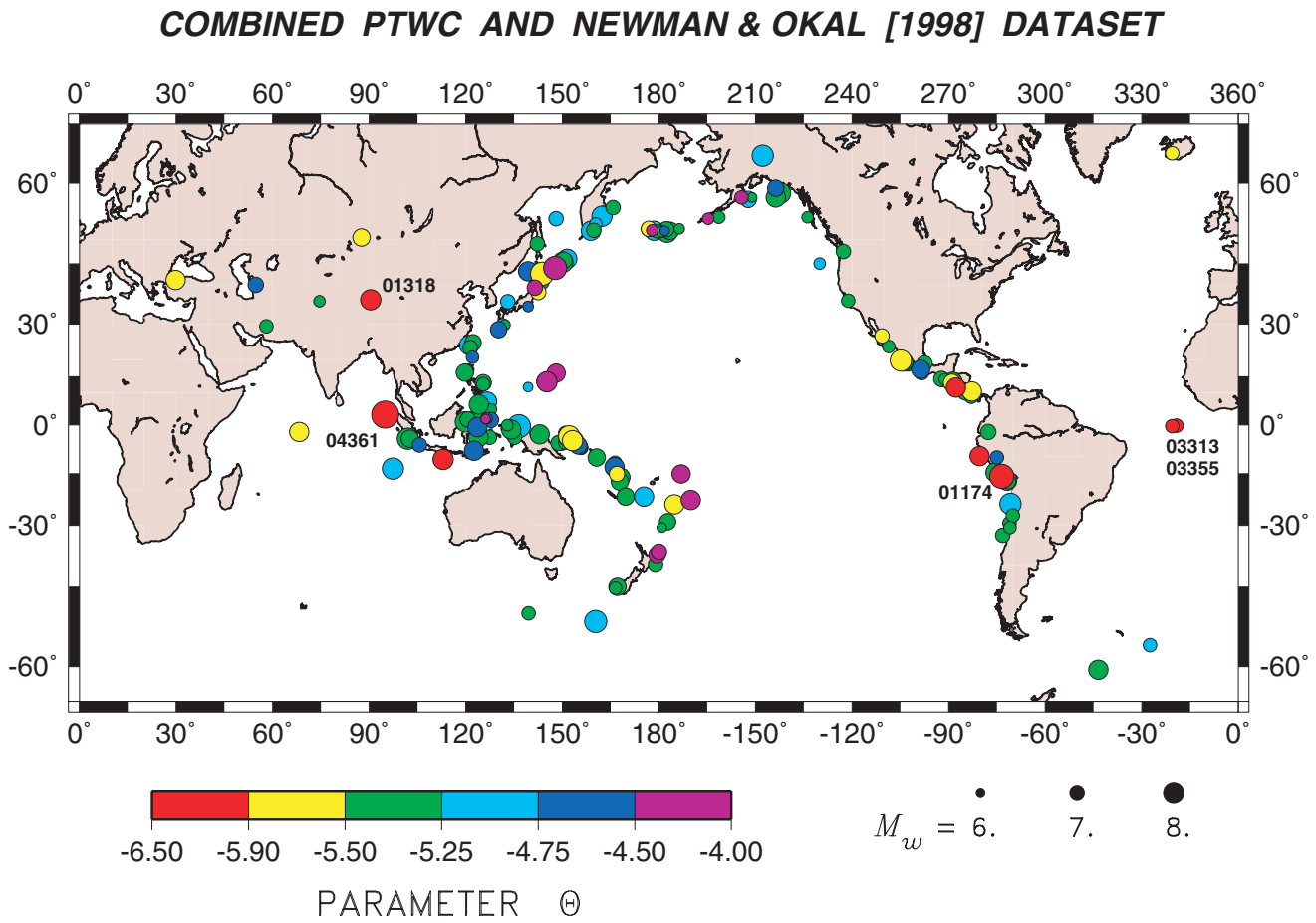

Figure 13. Combined dataset of events processed through the Θ algorithm, including the earthquakes analyzed by Newman and Okal (1998) and the 2004 Sumatra earthquake (see Appendix), color-keyed according to the event-averaged value of the parameter Θ. Note the absence of a definitive regional trend, as discussed by Okal and Newman (2001).

($T = 273$ sec) actually degrading their quality. An alternate algorithm consisting of retaining the average value of M_m measured on each record also provides generally excellent results, with the mean event-averaged value being -0.04 unit for the dataset of 5498 very-broadband records combining STS-1 and KS54000 instruments. A final combination of these two approaches, averaging over stations at each period and then retaining the maximum among such averages, also yields populations of residuals with $\overline{r_w}$ of only -0.10 ± 0.12 units (Fig. 8).

An implicit conclusion of our study is that the determination of an event-averaged M_m, in real time and under operational conditions, can and probably should ignore the contributions of the non-very-broadband, "other" stations, whose residuals, in general, are too large, especially at long periods and for small events. In other words and given the numerous stations now routinely contributing waveforms in real time, the benefits of incrementing the number of records for a given event no longer outweigh those of selecting the most performing instrumentation. Indeed, in all cases studied, we find a weak positive correlation between the event-averaged $\overline{r_w}$ and the number of stations N used in the computation (or between its absolute value, $|r_w|$, and N).

In the case of the 2001 Peruvian event and, in a somewhat similar vein, the proliferation of North American stations (incidentally, many of them equipped with non-very-broadband, "other" instrumentation) afflicted by a nodal radiation pattern and an unfavorable directivity function result in significantly deficient estimates of M_m under all averaging strategies. Paradoxically, the Preliminary Determination of Focal Mechanism (PDFM) algorithm run at Papeete (Reymond and Okal, 2000) performed better than Harvard's QUICK solution because it used fewer stations, thus retaining a better azimuthal balance (in addition to its use of Love waves, which stabilizes the solution when the number of stations is small). This would suggest that a more reliable event-averaged M_m could be obtained for large events from a subset of very-broadband stations carefully selected to provide homogeneous azimuthal coverage. Because the overwhelming majority of large, potentially tsunamigenic, interplate earthquakes have a focal geometry well predicted on the basis of plate tectonics theory, such subsets could be

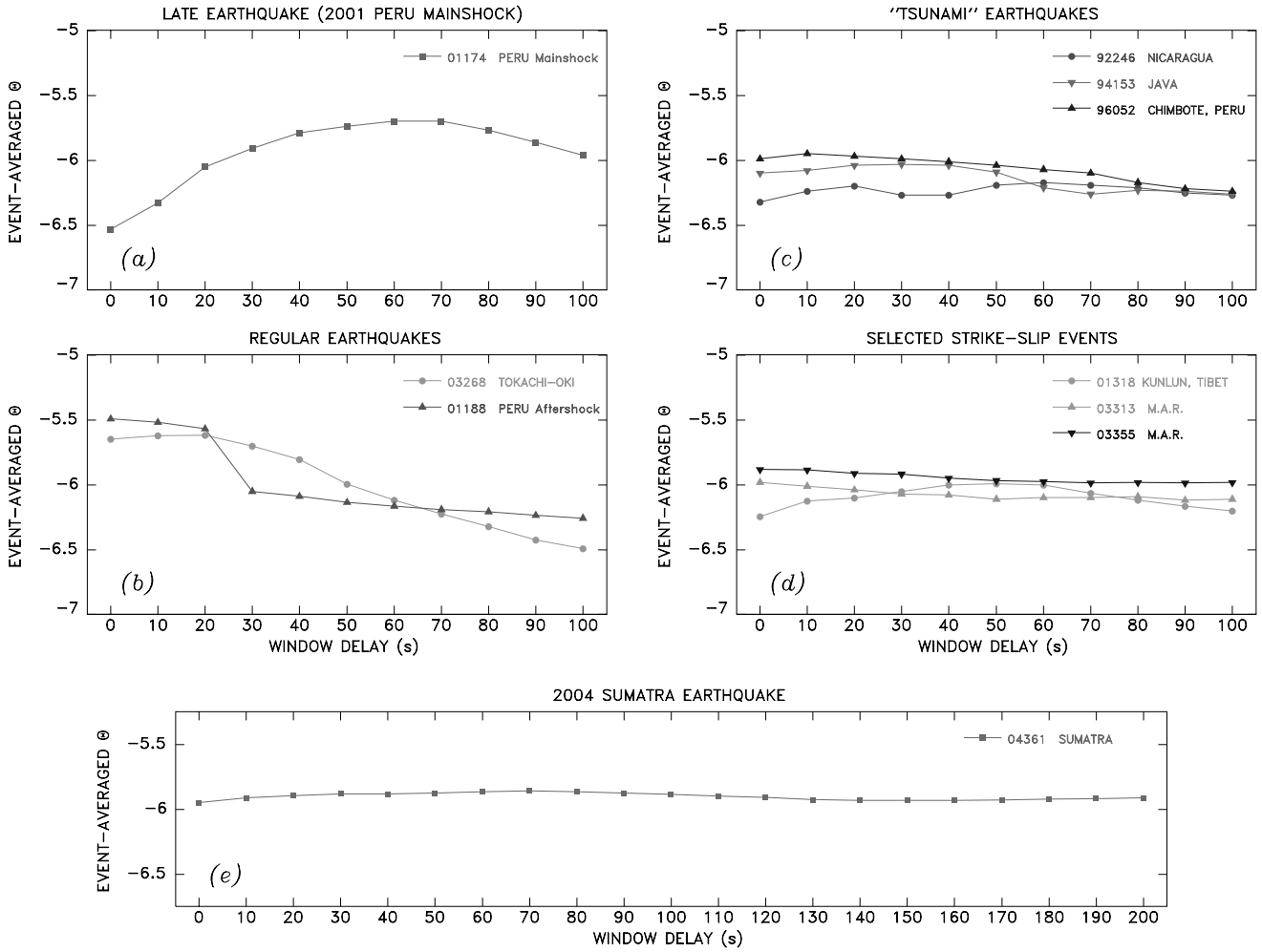

Figure 14. Variation of the parameter Θ for selected earthquakes as a function of the delay of the 70-sec-long time series window used in the algorithm. (a) Case of the late-developing 2001 Peruvian mainshock. (b) For regular earthquakes, the representative value of Θ is obtained without imposing a delay, but Θ falls when the window ceases to sample the *P* wave. (c) For the three "tsunami earthquakes" studied by Newman and Okal (1998) Θ is extremely deficient and essentially independent of window delay. (d) The behavior of Θ for three strike-slip earthquakes (on the Mid-Atlantic Ridge and Kunlun Fault) is similar to that of "tsunami earthquakes." (e) The 2004 Sumatra earthquake exhibits a remarkably constant behavior of Θ, suggesting a source duration of at least 350 sec.

preselected for various epicentral areas, and the implementation of this alternate algorithm automated in real time. Any difference between its results and those of the standard algorithms involving all reporting stations would then suggest a possible bias in the latter.

Our results also confirm the feasibility of determining in real time an estimate of the energy-to-moment ratio of distant earthquakes through the parameter Θ, and thus of identifying earthquakes featuring potential deviations in scaling laws, suggestive of anomalous behavior, and potentially enhanced tsunami excitation. However, our study shows, in the example of the 2001 Peruvian earthquake, that a deficient value of Θ obtained through the routine application of our standard algorithm must be confirmed by a more detailed investigation of the source, for example, through the use of a sliding window, before the slow character of an event can be recognized reliably. Finally, the routine processing of large earthquakes on a worldwide basis, including events posing no tsunami threat to the Pacific Basin, has allowed the identification of a few unsuspected sources featuring deficient Θ values, suggestive of anomalous characteristics in the morphology of their fault zones.

Acknowledgments

We thank Charles McCreery and Barry Hirshorn for their help and encouragement, NOAA/NWS for the use of their facilities, Ray Buland for discussion, and Paul Whitmore and the Alaska Tsunami Warning Center

for their contributions of seismic data to the effort. This research is supported in part by National Science Foundation Grant CMS-03-01054 (to E.A.O.). Maps were drafted using the GMT software of Wessel and Smith (1991). We thank many colleagues, too numerous to list individually, for sharing their preliminary results on the great Sumatra earthquake.

References

Bilek, S. L., and L. J. Ruff (2002). Analysis of the 23 June 2001 M_w = 8.4 Peru underthrusting earthquake and its aftershocks, *Geophys. Res. Lett.* **29,** no. 20, 1960, doi 10.1029/2002GL015543.

Boatwright, J., and G. L. Choy (1986). Teleseismic estimates of the energy radiated by shallow earthquakes, *J. Geophys. Res.* **91,** 2095–2112.

Bouchon, M., and M. Vallée (2003). Observation of long supershear rupture during the magnitude 8.1 Kunlunshan earthquake, *Science* **301,** 824–826.

Centroid Moment Tensor (CMT) Catalog, www.selsmology.harvard.edu/CMTsearch.html.

Dziewonski, A. M., G. Ekström, and N. Maternovskaya (2000). Centroid-moment tensor solutions for January-March 1999, *Phys. Earth Planet. Interiors* **118,** 1–11.

Fukao, Y. (1979). Tsunami earthquake and subduction processes near deep sea trenches, *J. Geophys. Res.* **84,** 2303–2314.

Geller, R. J. (1976). Scaling relations for earthquake source parameters and magnitudes, *Bull. Seism. Soc. Am.* **66,** 1501–1523.

Giovanni, M.K., S.L. Beck, and L. Wagner (2002). The June 23, 2001 Peru earthquake and the southern Peru subduction zone, *Geophys. Res. Lett.* **29,** no. 21, doi 10.1029/2002GL015774.

Hyvernaud, O., D. Reymond, J. Talandier, and E. A. Okal (1993). Four years of automated measurement of seismic moments at Papeete using the mantle magnitude M_m: 1987–1991, *Tectonophysics* **217,** 175–193.

Kanamori, H. (1972). Mechanisms of tsunami earthquakes, *Phys. Earth Planet. Interiors* **6,** 346–359.

Kanamori, H. (1977). The energy release in great earthquakes, *J. Geophys. Res.* **82,** 2981–2987.

Kanamori, H., and M. Kikuchi (1993). The 1992 Nicaragua earthquake: a slow tsunami earthquake associated with subducted sediment, *Nature* **361,** 714–715.

Kasahara, M., M. Ichiyanagi, H. Takahashi, M. Okayama, M. Takada, K. Katsumata, and Y. Motoya (2003). The 2003 Tokachi-Oki earthquake (M_w = 8.0), observed by local seismic and geodetic network in Hokkaido (abstract), *EOS Trans. AGU* **84,** no. 46, S52L–01.

Kikuchi, M., and Y. Yamanaka (2001). EIC Seismological Note Number 105, www.eic.eri.u-tokyo.ac.jp/EIC/EIC_news/105E.html.

Lin, A., M. Kikuchi, and B. Fu (2003). Rupture segmentation and process of the 2001 M_w = 7.8 Central Kunlun, China, earthquake, *Bull. Seism. Soc. Am.* **93,** 2477–2492.

Marshall, P. D., and P. W. Basham (1972). Discrimination between earthquakes and underground explosions using an improved M_s scale, *Geophys. J. R. Astr. Soc.* **28,** 431–458.

Newman, A. V., and E. A. Okal (1998). Teleseismic estimates of radiated seismic energy: the E/M_0 discriminant for tsunami earthquakes, *J. Geophys. Res.* **103,** 26,885–26,898.

Okal, E. A. (1990). M_m: a mantle wave magnitude for intermediate and deep earthquakes, *Pure Appl. Geophys.* **134,** 333–354.

Okal, E. A. (1992a). Use of the mantle magnitude M_m for the reassessment of the seismic moment of historical earthquakes. I. shallow events, *Pure Appl. Geophys.* **139,** 17–57.

Okal, E. A. (1992b). Use of the mantle magnitude M_m for the reassessment of the seismic moment of historical earthquakes. II. Intermediate and deep events, *Pure Appl. Geophys.* **139,** 59–85.

Okal, E. A., and A. R. Langenhorst (2000). Seismic properties of the Eltanin Transform System, South Pacific, *Phys. Earth Planet. Interiors* **119,** 185–208.

Okal, E. A., and A. V. Newman (2001). Tsunami earthquakes: the quest for a regional signal, *Phys. Earth Planet. Interiors* **124,** 45–70.

Okal, E. A., and L. M. Stewart (1982). Slow earthquakes along oceanic fracture zones: evidence for asthenospheric flow away from hot spots?, *Earth Plan. Sci. Lett.* **57,** 75–87.

Okal, E. A., and J. Talandier (1989). M_m: a variable period mantle magnitude, *J. Geophys. Res.* **94,** 4169–4193.

Okal, E. A., and J. Talandier (1990). M_m: Extension to Love waves of the concept of a variable-period mantle magnitude, *Pure Appl. Geophys.* **134,** 355–384.

Okal, E. A., and J. Talandier (1991). Single-station estimates of the seismic moment of the 1960 Chilean and 1964 Alaskan earthquakes, using the mantle magnitude M_m, *Pure Appl. Geophys.* **136,** 103–126.

Okal, E. A., L. Dengler, S. Araya, J. C. Borrero, B. Gomer, S. Koshimura, G. Laos, D. Olcese, M. Ortiz, M. Swensson, V. V. Titov, and F. Vegas (2002). A field survey of the Camaná, Peru tsunami of June 23, 2001, *Seism. Res. Lett.* **73,** 904–917.

Polet, J., and H. Kanamori (2000). Shallow subduction zone earthquakes and their tsunamigenic potential, *Geophys. J. Int.* **142,** 684–702.

Reymond, D., and E. A. Okal (2000). Preliminary determination of focal mechanisms from the inversion of spectral amplitudes of mantle waves, *Phys. Earth Planet. Interiors* **121,** 249–271.

Schindelé, F., D. Reymond, E. Gaucher, and E. A. Okal (1995). Analysis and automatic processing in near-field of the eight 1992–1994 tsunamigenic earthquakes: improvements in real-time tsunami warning, *Pure Appl. Geophys.* **144,** 381–408. 1995.

Scholz, C. H. (1982). Scaling laws for large earthquakes: consequences for physical models, *Bull. Seism. Soc. Am.* **72,** 1–14.

Shapiro, N. M., S. K. Singh, and J. Pacheco (1998). A fast and simple diagnostic method for identifying tsunamigenic earthquakes, *Geophys. Res. Lett.* **25,** 3911–3914.

Stein, S., and E. A. Okal (2005). Sumatra earthquake: gigantic and slow, *Nature* (in press).

Stewart, L. M., and E. A. Okal (1983). Seismicity and aseismic slip along the Eltanin Fracture Zone, *J. Geophys. Res.* **88,** 10,495–10,507.

Synolakis, C. E., J.-P. Bardet, J. C. Borrero, H. L. Davies, E. A. Okal, E. A. Silver, S. Sweet, and D. R. Tappin (2002). The slump origin of the 1998 Papua New Guinea tsunami, *Proc. R. Soc. London, Ser. A* **458,** 763–789.

Talandier, J., and E. A. Okal (1992). One-station estimates of seismic moments from the mantle magnitude M_m: the case of the regional field ($1.5° \leq \Delta \leq 15°$), *Pure Appl. Geophys.* **138,** 43–60.

Tanioka, Y., L. J. Ruff, and K. Satake (1997). What controls the lateral variation of large earthquake occurrence along the Japan Trench?, *The Island Arc* **6,** 261–266.

Tsuboi, S., K. Abe, K. Takano, and Y. Yamanaka (1995). Rapid determination of M_w from broadband P waveforms, *Bull. Seism. Soc. Am.* **85,** 606–613.

Tsuboi, S., P. M. Whitmore, and T. J. Sokolowski (1999). Application of M_{wp} to deep and teleseismic earthquakes, *Bull. Seism. Soc. Am.* **89,** 1345–1351.

Vassiliou, M. S., and H. Kanamori (1982). The energy release in earthquakes, *Bull. Seism. Soc. Am.* **72,** 371–387.

Wang, C.-Y., Z.-F. Ding, and W. W. Chan (2003). High-resolution exploration of the Kunlun Fault, China: implications from the M_w = 7.8 Kunlun earthquake (abstract), *Seism. Res. Lett.* **74,** 242.

Wessel, P., and W. H. F. Smith (1991). Free software helps map and display data, *EOS Trans. AGU* **72,** 441, 445–446.

Preliminary Analysis of the Great Sumatra Earthquake (26 December 2004)

We complement this study by data pertaining to the great 2004 Sumatra earthquake. At the time of writing (17 January 2005), a preliminary moment (3.95×10^{29} dyne cm or $M_w \approx 9.0$) has been released by the Harvard CMT project, using an algorithm specially adapted to the exceptional size

of the event, the inversion being performed at $T = 300$ sec. Residuals r_w will be computed relative to this estimate, even though preliminary observations from aftershock distribution, tsunami simulation, and radial mode analysis (P.-Y. Le Traon, V. V. Titov, D. Arcas, J. Park, personal comm., 2005) would suggest that the static moment of the earthquake could be even larger. Indeed, we document here that the earthquake exhibits anomalous slowness, its parameter Θ being comparable with those of the 1994 Java and 1996 Chimbote, Peru, events.

M_m Measurements

In view of the size of the event, the M_m algorithm was altered to include measurements down to $f = 2.5$ mHz (in practice, up to $T = 409.60$ sec), which can be taken as the limit of the observation of Rayleigh waves as an essentially continuous spectrum. The M_m dataset for the Sumatra event comprises 2197 measurements at 77 stations and 29 periods. The residuals are expectedly strongly negative, featuring $\overline{r_w} = -0.63 \pm 0.29$ for the full dataset, with all classes of instruments equally affected ($\overline{r_w} = -0.62, -0.73, -0.55$, and -0.55 for the STS-1, KS-54000, STS-2, and "other" systems, respectively). We interpret this as attributable to the strong destructive interference at all frequencies resulting from the exceptional length and duration of the source. Even at the longest period, $T = 410$ sec, the average residual remains negative, but acceptable (-0.15 on 71 stations). Surprisingly, the STS-2 and "other" systems fare better ($\overline{r_w} = -0.02$ and $+0.03$, respectively) than the very-broadband STS-1 and KS-54000 ones ($\overline{r_w} = -0.22$ and -0.16, respectively). We attribute this observation to the exceptional signal-to-noise ratio at this ultralong period, which overrides the poorer response of the STS-2 and "other" systems; as suggested by the Θ measurements and other evidence (see previously), the earthquake is expected to last at least 300 sec, and more realistically 400 sec. As such, all measurements including those at the longest periods ($T = 410$ sec) are expected to be contaminated by destructive interference caused by source directivity, and the better performance of the STS-2 and "other" families may be the result of their concentration at the least unfavorable azimuth, namely on the North American continent.

Finally, we note that the original M_m algorithm, which consists of retaining at each station the largest value of M_m, once extended to $T = 410$ sec, yields a station-averaged residual of only $\overline{r_w} = -0.11$, which must be regarded as acceptable and, in particular, clearly establishes the exceptionally large nature of the event.

Θ Measurements

Measurements of estimated energy E^E were obtained at 30 stations ranging from 33° to 89° and were interpreted in terms of the parameter Θ by using the Harvard moment $M_0 = 3.95 \times 10^{29}$ dyne cm. The initial algorithm yielded an average $\Theta = -6.60$, which is clearly biased by the use of a window significantly shorter than any estimate of the duration of the event. For this reason, we extended the window of analysis to a duration of 150 sec. this figure may still fall short of the duration of the earthquake source, but using longer windows would result in systematic contamination of the waveform with phases such as *PcP* (at most distances) and *PP* (at all distances). This procedure resulted in $\bar{\Theta} = -5.95 \pm 0.36$ (see inverted triangles on Fig. 13), comparable with its value for the 1996 Chimbote, Peru, earthquake.

The slow character of the source was further established by using the sliding window approach described in The Slowness Parameter Θ section over a sliding interval of 200 sec. As shown on Figure 14e, the result is an essentially constant value of Θ (-5.95 ± 0.03), which indicates that the sliding window does sample the source continuously, in other words, that the source lasts at least 350 sec. This is in general agreement with the preliminary evidence mentioned previously, but it is significantly longer than the ~150 sec predicted by scaling laws (Geller, 1976) for the moment proposed by Harvard. We conclude that the earthquake exhibits significant slowness, which suggests that the Harvard moment computed at 300 sec may underestimate the static value.

Note Added to Proof

This trend toward an exceptionally large and slow source has recently been confirmed by a study of the Earth's free oscillations excited by the earthquake (Stein and Okal, 2005).

Pacific Tsunami Warning Center, NOAA
91-270 Fort Weaver Road
Ewa Beach, Hawaii 96706
(S.A.W.)

Department of Geological Sciences
Northwestern University
Evanston, Illinois 60201
(E.A.O.)

Manuscript received 14 June 2004.